MODELING THE CORROSIVE EFFECTS OF VARIOUS MAGNESIUM ALLOYS EXPOSED TO TWO SALTWATER ENVIRONMENTS

H.J. Martin, C. Walton, J. Danzy, A. Hicks, M.F. Horstemeyer, P.T. Wang

Center for Advanced Vehicular Systems (CAVS), Mississippi State University, Box 5405, Mississippi State, MS 39762, USA

Keywords: Magnesium Alloy, Pitting Corrosion, Intergranular Corrosion, Modeling of Corrosion

Abstract

The use of magnesium within the automotive industry is limited by its corrosion rate in the presence of saltwater. By adding various elements, the magnesium microstructure and corrosion rate can be altered. In the Center for Advanced Vehicular Systems at Mississippi State University, a model is being developed to elucidate the total corrosion of magnesium alloys and is comprised of general corrosion and pitting corrosion, respectively, as shown below:

$$\phi = \phi_{gc} + \phi_{IC} \tag{1}$$

where pitting corrosion is based on the pit number density, pit surface area, and a nearest neighbor distance function, respectively, as shown below:

$$\phi_{IC} = \eta_p v_p C \tag{2}$$

The exposure environment resulted in differences in the amount of pit nucleation, in the size of the pits formed, and in the rate of coalescence. Time also affected the surface characteristics, as general corrosion began degrade the number and size of the pits. The research presented here will cover the model development, calibration, and validation.

Introduction

Magnesium has a high corrosion rate as compared to aluminum or steel, relegating its role in the automotive and aerospace industries in places that are unexposed to the environment [1-3]. In an effort to improve the corrosion resistance of magnesium, various elements are added, including aluminum, zinc, manganese, and rare earth elements [2, 4-8].

The addition of aluminum, up to 10%, has been shown to affect the corrosion resistance of magnesium [2]. Aluminum, which is present in the β-phase precipitate, appearing as $Mg_{17}Al_{12}$, leads to improved corrosion resistance when the β-phase is continuous and finely divided [2, 9-11]. However, the same β-phase precipitate can lead to the creation of micro-galvanic cells, thereby decreasing the corrosion resistance, when the β-phase is small and unconnected [2, 9-11].

In addition to the addition of aluminum, the presence of rare earth elements can affect the corrosion properties and mechanical properties of magnesium [4-8]. The formation of meta-stable rare earth element – containing phases along the grain boundaries improves the creep properties of magnesium and can also improve corrosion resistance due to trace amounts of the rare earth elements in the passive films formed during atmospheric exposure [6-8, 12]. The addition of the rare earth elements also shifts the location of pitting corrosion, from along the magnesium grain – eutectic boundary to the interior of the magnesium grain, resulting in unaffected rare earth intermetallic regions [7, 13].

The presence of alloying elements is not the only consideration when dealing with corrosion. The formation method, whether it is extrusion or casting, plays a significant role in the corrosion properties of magnesium alloys. Casting results in the formation of an as-cast "skin", with very small grains, which increases the corrosion resistance of magnesium, up to ten-fold higher than the bulk material [9, 14]. Since extrusion removes this as-cast skin, and does not allow the formation of another skin, extrusion can negatively affect the corrosion resistance of magnesium.

While the addition of elements to magnesium can increase the corrosion resistance of magnesium, currently, there are no available models to determine if the addition of certain elements will improve corrosion resistance. Models designed for stainless steel and aluminum attempt to quantify the causes of pitting, such as diffusion, energy, pH, and corrosion potential, but involve the use of a current to initiate the corrosion [15-22]. In addition, the only available model for magnesium requires a current to produce a polarization curve to predict galvanic corrosion, which is not applicable to this research [23]. The goal of this research, then, is to study various magnesium alloys in as-cast or extruded form in order to develop a model that accurately describes pit nucleation, pit growth, and pit coalescence.

Materials and Methods

Testing

Twelve AZ61 coupons (2.54 cm x 2.54 cm x varying thicknesses) were cut from an extruded crash rail provided by Ford using a CNC Mill (Haas, Oxnard, CA). Twelve AZ31 coupons (cm x cm x cm) were cut from extruded sheets using a vertical band saw (MSC Industrial Supply Company, Columbus, MS). Twelve AM60 coupons (2.54 cm x 2.54 cm x varying thicknesses) were cut from as-cast control arms using a vertical band saw. Twelve AE44 coupons (2.54 cm x 2.54 cm x varying thicknesses) were cut from an as-cast engine cradle provided by Meridian Technologies using a vertical band saw. The coupon surfaces were left untreated to test the corrosion effects on the extruded AZ61 and AZ31 magnesium alloys and on the as-cast AM60 and AE44 magnesium alloys.

Two different test environments were used in this study: salt spray testing and immersion. For salt spray testing, a Q-Fog CCT (Q-Panel Lab Products, Cleveland, OH) was used to cycle through three stages set at equal times, including a 3.5 wt.% NaCl spray at 35°C, 100% humidity using distilled water at 35°C, and a drying purge at 35°C. For immersion testing, an aquarium with an aeration unit was filled with 3.5 wt.% NaCl at room temperature. For both tests, the six coupons per test environment were hung at 20° to the horizontal, as recommended by ASTM B-117 [24]. The coupons were exposed to the test environment for 1 h, removed, rinsed with distilled water to remove excess salt, and dried. Following the profilometer analysis, the coupons were then placed

back into the test environment for an additional 3 h, an additional 8 h, an additional 24 h, and another 24 h. These times allowed for a longitudinal study to follow pit growth and surface changes over time, where $t_0 = 0$, $t_1 = 1$ h, $t_2 = 4$ h, $t_3 = 12$ h, $t_4 = 36$ h, and $t_5 = 60$ h. Between analyses and environmental exposures, the coupons were stored in a desiccator to ensure that no further surface reactions occurred.

Analysis

Following each time exposure, the coupons were analyzed using optical microscopy and laser profilometry. The coupons were weighed prior to testing and following each exposure on two different scales and an average was taken. Four thickness measurements were taken on each sample prior to and following the test. Because the coupons were cut from an engine cradle, the thicknesses of the coupons varied from side to side, meaning an average was taken per coupon based on the four measurements. Measurements for all figures were averaged from the data with error bars based on one standard deviation.

Optical microscopy with an inverted light was used to take multiple images of the resulting surface at 5x magnification and 10x magnification (Axiovert 200M Mat, Carl Zeiss Imaging Solutions, Thornwood, NY). The 5x magnification images were combined and then analyzed using the ImageAnalyzer (v. 2.1-2) provided by Mississippi State University to determine the number of pits, the pit surface area, the nearest neighbor radius, and the intergranular corrosion area fraction necessary for the development of a corrosion model not detailed in this paper but previously outlined by Horstemeyer *et al.* [25]. The 10x magnification was used to pictorially show the changes over the six cycles. Laser profilometry was used to scan a 1 mm by 1 mm area on two coupons per environment following each test cycle (Talysurf CLI 2000, Taylor Hobson Precision Ltd, Leicester, England). The resulting 2-D and 3-D images were used to document the changes in the pit characteristics due to the different test environments over the six cycles (Talymap Universal, v. 3.18, Taylor Hobson Precision Ltd, Leicester, England). Data was collected based on fourteen pits within each 1 mm by 1 mm area, for a total of twenty-eight data points per environment per cycle.

Results

Figures 1 and 2 show the average weight and thickness loss, respectively, over the five exposure times for the immersion and salt spray surfaces on the various magnesium alloys being compared. As one can see, all surfaces follow similar logarithmic trends for weight loss (Figure 1) and thickness loss (Figure 2).

Figure 3 shows the pit number density over the five exposure times for the immersion and salt spray surfaces on the various magnesium alloys being compared. As one can see, all surfaces followed second-order polynomial trends. The AZ61 surfaces showed the highest amount of pit formation as compared to the other surfaces, while the as-cast AM60 surfaces showed the lowest amount of pit formation. In addition, all immersion surfaces had higher pit number densities as compared to the respective salt spray surface.

Figure 4 shows the changes in the pit area, which is the 2-D area covered by the pits as seen by micrographs for the immersion and salt spray surfaces on the various magnesium alloys being

compared. As with pit number density, the most surfaces followed a second-order polynomial, with the highest pit area occurring on the AE44 immersion surface. Also notice that the AZ31 surface was divided by 10 so as not to compress the data on the the y-axis, making the three other surfaces indistinguishable. In addition, there was no decrease in pit area on the AZ61 salt spray surface or either AZ31 surfaces, which increased until the end of the experiment. The smallest pit area occurred on the AM60 as-cast surfaces.
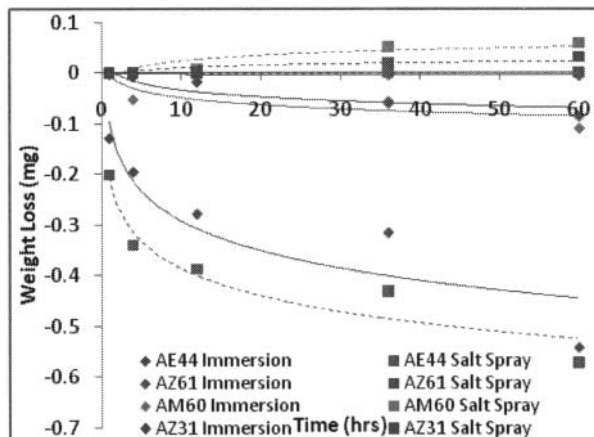

Figure 1: Average weight loss of various magnesium alloys based on test environment over 60 h. Notice that all surfaces followed logarithmic trends.
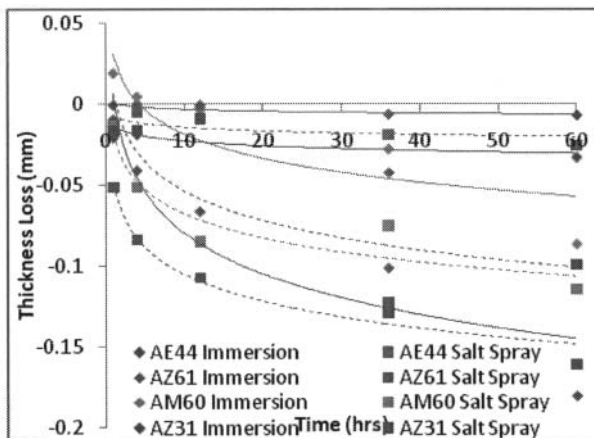

Figure 2: Average thickness loss of various magnesium alloys based on test environment over 60 h. Notice that all surfaces followed logarithmic trends.

Figure 5 shows the changes in the nearest neighbor distance, which is the distance between two pits, for the immersion and salt spray surfaces on the various magnesium alloys being compared. As with the pit number density and the pit area, the surfaces followed second-order polynomial trends, although in reverse of the pit number density and pit area. The extruded AZ61 surfaces showed the smallest nearest neighbor distance while the as-cast AM60 surfaces showed the largest nearest neighbor distance.

Figure 6 shows the intergranular corrosion area fraction (ICAF), which is the fraction of the surface that shows the corrosion that

occurs in the β-phase precipitate phase of the alloy, for the immersion and salt spray surfaces on the various magnesium alloys being compared. All surfaces follow logarithmic trends, with the highest ICAF occurring on the as-cast AE44 surfaces.
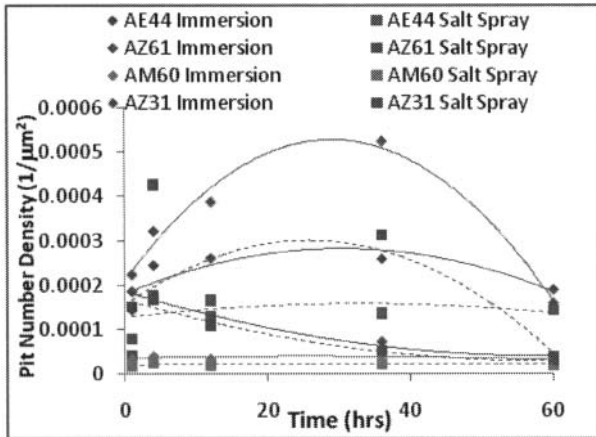

Figure 3: Pit number density of various magnesium alloys based on test environment over 60 h. Notice that all surfaces followed second-order polynomial trends. Also notice that all immersion surfaces had higher pit number densities as compared to the respective salt spray surface.
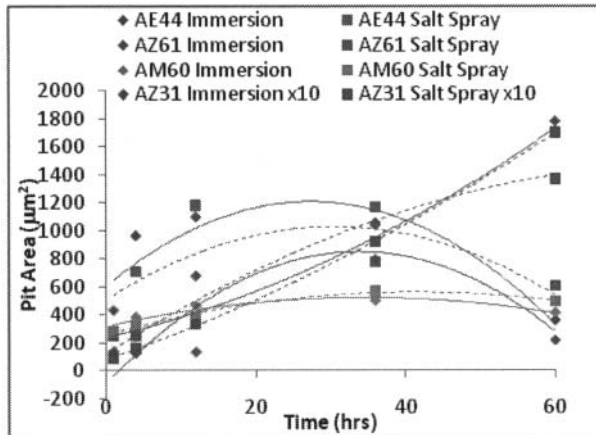

Figure 4: In-plane pit area of various magnesium alloys based on test environment over 60 h. Notice that all surfaces followed second-order polynomial trends. Also notice that the extruded AZ31 surfaces had the largest pit area, which was divided by 10 to ensure all data could be seen. Notice also that the as-cast AM60 surfaces had the smallest pit area. In addition, there was no decrease in pit area on the extruded AZ61 salt spray surface.

Discussion

Total corrosion includes general corrosion, which occurs when water reacts with a magnesium surface to create a $Mg(OH)_2$ film and H_2 gas, and pitting corrosion, which occurs when chloride ions from salt water initiate and maintain pit formation on the magnesium surface [3]. At Mississippi State University, a model is currently being developed that incorporates general corrosion and pitting corrosion, as shown below:

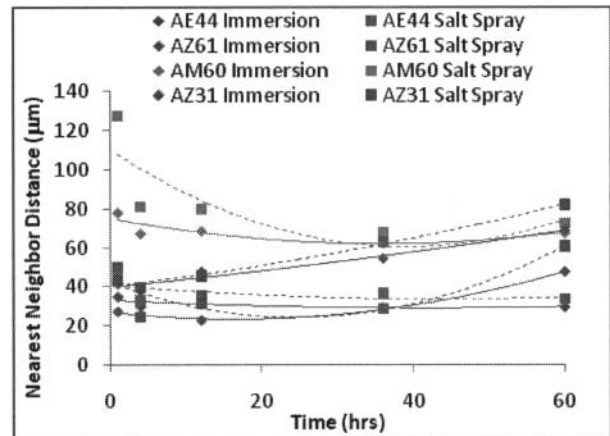$$\phi = \phi_{gc} + \phi_{IC} \tag{1}$$

Figure 5: Nearest neighbor distance of various magnesium alloys based on test environment over 60 h. Notice that all surfaces followed second-order polynomial trends. Also notice that the as-cast AM60 surfaces had the largest nearest neighbor distance while the extruded AZ61 surfaces had the smallest nearest neighbor distance.
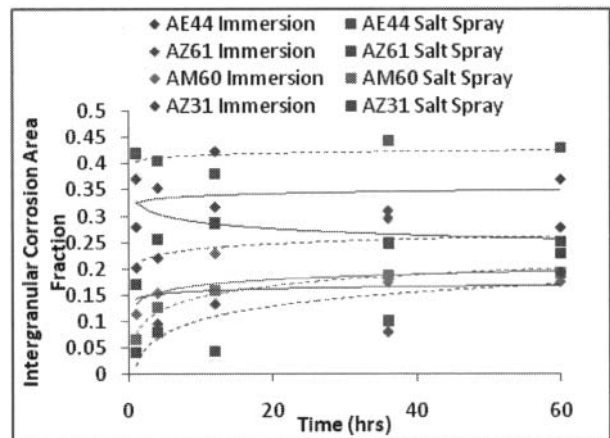

Figure 6: Intergranular corrosion area fraction of various magnesium alloys based on test environment over 60 h. Notice that all surfaces followed logarithmic trends. Also notice that the as-cast AE44 surfaces had the largest intergranular corrosion area fraction.

General corrosion (ϕ_{gc}) is measured by the weight loss and thickness loss of the magnesium coupons, which is only minimally affected by pitting corrosion. Pitting corrosion (ϕ_{IC}), however, is extremely detrimental to materials, as it may not be detected until it penetrates the entire surface since it does not reduce the weight or thickness of the material [3]. Pitting corrosion can be measured by the nucleation, growth, and coalescence of the pits, as shown below:

$$\phi_{IC} = \eta \, v_p c \tag{2}$$

where η is the pit number density, v is the pit area, and c is a function of the nearest neighbor distance and the intergranular corrosion area fraction (ICAF).

When looking at general corrosion, more weight loss is seen on the immersion surfaces as compared to the salt spray surfaces, except with respect to the as-cast AE44 surfaces (Figure 1). Because the samples in the immersion environment are continuously surrounded by salt containing water, more water can react with the surface, leading to more weight loss as magnesium is removed from the surface. When looking at the salt spray surfaces, which are exposed first to salt containing water, then to 100% humidity, and then to a dry phase, weight loss is not as significant, since there is no continuous exposure to water, meaning there is no continuous general corrosion ongoing. However, more thickness loss is seen on the salt spray surfaces as compared to the immersion surfaces (Figure 2). This is not expected, as one would expect that thickness loss would follow weight loss. The difference in thickness and weight loss, though, can be attributed to the way measurements were taken. Weight loss used a scale, meaning the entire coupon was measured, while thickness loss was taken using calipers, meaning only the edges of the coupons were measured. This difference can account for the difference in thickness loss, as cleaning the samples after each corrosion period removed significant pit debris and salt on the salt spray samples. While both samples hung at 20°, the samples exposed to the cyclical salt spray experienced a collection of pit debris and salt along the edges of the samples, due to the drying phase. This debris led to higher pitting corrosion along the edges, which were measured with the calipers. Because there was no collection of salt or pit debris along the edges of the immersion samples, extra pits could not form meaning the thickness was unaffected by the debris.

General corrosion, however, is only part of the model. The other portion of the model is pitting corrosion, which relates pit number density, pit area, nearest neighbor distance, and intergranular corrosion area fraction (ICAF). The first three values are highly interrelated. Pit number density and pit area are related because at the number of pits increase, the area covered by the pits increase. However, the pits can grow without the pit number increasing, meaning that pit area is not solely related to pit number density. Pit number density and nearest neighbor distance are also related, because as the pit increase in number, the distance between them decreases. Lastly, the pit area and nearest neighbor distance are related because as the pits grow in size, the distance between them decreases.

These relationships are demonstrated in Figures 3-5. As the pit number density increases, so does the pit area, while the nearest neighbor distance decreases. The pit number density begins to decrease prior to pit area decreasing, as the pits can grow in size even when the pit number density decreases. In addition, the nearest neighbor distance decreases even as pit number density decreases, due to the slight growth in pit area. Once pit area begins to decrease, and pit number density continues to decrease, the nearest neighbor distance begins to increase.

The differences seen in pit number density (Figure 3) can be attributed to the environment to which the magnesium is exposed, the form of magnesium, and the type of magnesium alloy. When it comes to the salt spray environment, fewer pits are seen on all surfaces as compared to the immersion surface. This is due to continuous exposure of chloride ions to the immersion surfaces, allowing the chloride ions to continually attack and pit the surfaces. However, chloride ions are only present on the salt spray surfaces for a limited time, meaning that the surfaces can only pit when the chloride ions are present, resulting in lower numbers of pits forming. When comparing the form of magnesium, one can see that the extruded magnesium experienced much higher amounts of pit nucleation than the as-cast magnesium. This is due to the presence of an as-cast skin increasing the corrosion resistance on the as-cast alloys [9, 14]. This skin was removed during the extrusion process, meaning that the extruded magnesium can more easily corrode. Finally, the type of magnesium places a role in the formation of pitting. The higher the amount of aluminum, up to 10%, the higher the corrosion resistance [2]. When comparing the two as-cast materials, the lower pit nucleation corresponded with the higher percentage of aluminum, meaning that aluminum played a higher role in corrosion resistance than either zinc or rare earth elements.

The differences seen in pit area (Figure 4) can also be attributed to the environment to which the magnesium is exposed, the form of magnesium, and the type of magnesium alloy. When looking at the environments, larger pits were seen on the AZ61 and AM60 salt spray surfaces as compared to the immersion surfaces. AE44 and AZ31 showed higher pit areas on the immersion surface as compared to the salt spray surface. The higher pit areas on the salt spray surfaces are due to the presence of pit debris covering the formed pits during the humidity and drying phases. Pit growth is considered autocatalytic, so once it starts, it continues unabated [1]. When pit debris covers the pit, as it does on the salt spray surfaces due to the inability of the humidity and drying phases to remove the pit debris, the pits can continue to grow without general corrosion interfering. When the pit debris is removed, either during the salt spray phase where water is present or during the cleaning process, the larger pits can be seen. While there is a minimal difference in pit area on the AZ31 surfaces, a difference is seen with the AE44 surface, though, because of the shift in corrosion location. When rare earth elements are present, corrosion shifts to the center of the grain and away from the intergranular region [7, 13]. This shift encourages general corrosion and pitting corrosion to "work together", thereby increasing the pit area on the immersion surface. In addition to the environment, though the form of magnesium plays a role in the pit area. The as-cast AM60 material has a smaller pit area on both environments as compared to the extruded AZ61 material. This again can be attributed to the as-cast skin on the AM60 material, which prevents pits from growing due to the small grain size. The extruded AZ61 material does not possess the as-cast skin, meaning that the pits can grow more easily. Again, AE44 does not follow this line, again likely due to the shift in pit formation location. Even though an as-cast skin exists on the AE44 material, the pits form within the magnesium grain. General corrosion works alongside pitting corrosion to degrade the magnesium grains, which grow together, indicating an increase in pit area. The magnesium alloy also appeared to play a role in the pit area, with the smallest pit area occurring on the as-cast AM60 material, the largest pit area occurring on the as-cast AE44 material, and the middle pit area occurring on the extruded AZ61 and AZ31 materials. One could suspect that the presence of manganese affected the growth of the pits differently than the presence of either zinc or rare earth elements, but there is not currently enough alloys to accurately confirm this suspicion.

When it comes to the nearest neighbor distance (Figure 5), as previously mentioned, the pit number density and pit area greatly affect the nearest neighbor distance. The higher the pit number density and the larger the pits, the smaller the nearest neighbor

distance. When comparing the environments, since there are more pits formed on the immersion environments, the pits are closer together on the immersion surfaces. When comparing forms of magnesium, the as-cast AE44 surface and the extruded AZ61 surface had similar nearest neighbor distances because of the combination of pit area and pit number density, as did the as-cast AM60 surface and the extruded AZ31 surface. Since the AZ61 surface had a higher pit number density but smaller pit areas as compared to the AE44 surface, the values combine to cause the nearest neighbor distance to appear similar. However, the as-cast AM60 magnesium alloy had the smallest pit number density and the smallest pit areas, the AM60 nearest neighbor distance would be the largest, or furthest apart. In addition, the extruded AZ31 magnesium alloy experienced a decrease in pit number density and an increase in pit area, meaning that the nearest neighbor distance was more influenced by the size of the pits instead of the number of pits. The pit area of AZ31, which was 10x higher than the other pit areas, ensured that the nearest neighbor distance started close and gradually increased, as the large pits incorporated other pits, increasing the distance between the remaining pits.

The intergranular corrosion area fraction (ICAF) is another measure of the coalescence of the pits, because as the pits that form along the intergranular boundary grow together, they eventually grew into each other, forming one long narrow pit. The type of magnesium alloy affected the ICAF much more than either the environment or the form of the magnesium alloy (Figure 6). When comparing the extruded AZ61 alloy with the as-cast AM60 alloy, once can see that the environment affected on the beginning of the ICAF, but by the end of the experiment time, the ICAF had merged between the salt spray and immersion environments. In addition, there was very little difference between the AM60 and AZ61 ICAF. However, there was a significant difference between AM60, AZ61, AZ31, and AE44. The difference is due to the presence of aluminum influencing the corrosion of AZ31 and the rare earth elements and the as-cast skin influencing the corrosion of AE44. For AZ31, there was 3% less aluminum in the magnesium alloy. Since aluminum, increasing to 10%, has been shown to increase the corrosion resistance of magnesium [2], it stands to reason that the lower percentage of aluminum in AZ31 would allow more intergranular corrosion. For AE44, both the alloying elements and the skin contributed to the formation of intergranular corrosion. Since rare earth elements switch corrosion from along the intergranular boundary to the interior of the magnesium grain [7,13] and the as-cast skin results in very small grains, the presence of ICAF means that the grains were degrading and connecting along the intergranular boundary. If there was no as-cast skin, meaning the grains were much larger, there is a chance that the ICAF would have been more in line with the AM60 and AZ61 samples. In addition to the differences caused by the presence of rare earth elements and the as-cast skin, the environment contributed to a difference in ICAF, with the immersion surface experiencing less intergranular corrosion than the salt spray surface. This difference can be contributed to general corrosion, which removed the intergranular boundaries that were left by the pitting and destruction of the magnesium grains. With general corrosion removing, or lowering, the intergranular boundaries, intergranular corrosion may not have been accurately quantified.

Conclusions

Four magnesium alloys in two forms, as-cast AE44, as-cast AM60, extruded AZ61, and extruded AZ31 were examined in two corrosive environments, immersion and salt spray. General corrosion characteristics, weight loss and thickness loss, as well as surface characteristics, pit number density, pit area, nearest neighbor distance, and ICAF, were quantified over 60 hours. The most heavily corroded magnesium alloy, determined by combining general and pitting corrosion, was AZ61, followed by AE44, AZ31, and AM60, respectively. When comparing environments, more pits formed on all surfaces exposed to the immersion environment, while the pits were larger on the salt spray environments.

References

[1] M.G. Fontana, Corrosion Principles, in: M.G. Fontana (Eds.), Corrosion Engineering, McGraw-Hill, Boston, 1986, pp. 12-38.

[2] G. Song, A. Atrens, "Understanding Magnesium Corrosion – A Framework for Improved Alloy Performance", Advanced Engineering Materials 5 (2003) 837-858.

[3] BA Shaw, Corrosion Resistance of Magnesium Alloys, in: L.J. Korb, ASM (Eds.), ASM Handbook, Vol. 13A: Corrosion, Ninth Ed., ASM International Handbook Committee, Metals Park, 2003, pg. 692.

[4] J.D. Majumdar, R. Galun, B. Mordike, I. Manna, "Effect of laser surface melting on corrosion and wear resistance of a commercial magnesium alloy", Materials Science and Engineering A, 361 (2003) 119-129.

[5] C. Blawert, E.D. Morales, W. Dietzel, K.U. Kainer, "Comparison of Corrosion Properties of Squeeze Cast and Thixocast MgZnRE Alloys", Materials Science Forum, 488-489 (2005) 697-700.

[6] W. Liu, F. Cao, L. Chang, Z. Zhang, J. Zhang, "Effect of rare earth element Ce and La on corrosion behavior of AM60 magnesium alloy", Corrosion Science, 51 (2009) 1334-1343.

[7] W. Liu, F. Cao, L. Zhong, L. Zheng, B. Jia, Z. Zhang, J. Zhang, "Influence of rare earth element Ce and La addition on corrosion behavior of AZ91 magnesium alloy", Materials and Corrosion, 60 (2009) 795-803.

[8] Y.L. Song, Y.H. Liu, S.R. Yu, X.Y. Zhu, S.H. Wang, "Effect of neodymium on microstructure and corrosion resistance of AZ91 magnesium alloy", Journal of Materials Science, 42 (2007) 4435-4440.

[9] G. Song, "Recent Progress in Corrosion and Protection of Magnesium Alloys", Advanced Engineering Materials, 7 (2005) 563-586.

[10] M.C. Zhao, M. Liu, G. Song, A. Atrens, "Influence of pH and chloride ion concentration on the corrosion of Mg alloy ZE41", Corrosion Science, 50 (2008) 1939-1953.

[11] G. Song, A. Atrens, X. Wu, B. Zhang, "Corrosion behavior of AZ21, AZ501, and AZ91 in sodium chloride", *Corrosion Science*, 40 (1998) 1769-1791.

[12] Y.L. Song, Y.H. Liu, S.H. Wang, S.R. Yu, X.Y. Zhu, "Effect of cerium addition on microstructure and corrosion resistance of die cast AZ91 magnesium alloy", *Materials and Corrosion*, 58 (2007) 189-192.

[13] N. Birbilis, M.A. Easton, A.D. Sudholz, S.M. Zhu, M.A. Gibson, "On the corrosion of binary magnesium-rare earch alloys", *Corrosion Science*, 51 (2009) 683-689.

[14] G. Song, A. Atrens, M. Dargusch, "Influence of microstructure on the corrosion of diecast AZ91D", *Corrosion Science*, 41 (1998) 249-273.

[15] S.P. White, G.J. Weir, N.J. Laycock, "Calculating chemical concentrations during the initiation of crevice corrosion", *Corrosion Science*, 42 (2000) 605-629.

[16] R.M. Pidaparti, A. Puri, M.J. Palakal, A. Kashyap, "Two-dimensional Corrosion Pit Initiation and Growth Simulation Model," *Computers, Materials, and Continua*, 2 (2005) 65-75.

[17] R.M. Pidaparti, L. Fang, M.J. Palakal, "Computational simulation of multi-pit corrosion process in materials", *Computational Materials Science*, 41 (2008) 255-265.

[18] N.J. Laycock, J.S. Noh, S.P. White, D.P. Krouse, "Computer simulation of pitting potential measurements", *Corrosion Science*, 47 (2005) 3140-3177.

[19] N.J. Laycock, J. Stewart, R.C. Newman, "The initiation of crevice corrosion in stainless steel", *Corrosion Science*, 39 (1997) 1791-1809.

[20] L. Li, X. Li, C. Dong, Y. Huang, "Computational simulation of metastable pitting of stainless steel", *Electrochimica Acta*, 54 (2009) 6389-6395.

[21] T. Johnsen, A. Jossang, T. Jossang, P. Meakin, "An experimental study of the quasi-two-dimensional corrosion of aluminum foils and a comparision with two-dimensional computer simulations", *Physica A*, 242 (1997) 356-276.

[22] B. Malki, B. Baroux, "Computer simulation of the corrosion pit growth", *Corrosion Science*, 47 (2005) 171-182.

[23] J.X. Jia, G. Song, A. Atrens, "Experimental Measurement and Computer Simulation of Galvanic Corrosion of Magnesium Coupled to Steel", *Advanced Engineering Materials*, 9 (2007) 65-74.

[24] ASTM B117 - 07a (2007) Standard Practice for Operating Salt Spray (Fog) Apparatus, Vol. 03.02, 2007.

[25] M.F. Horstemeyer, J. Lathrop, A.M. Gokhale, M. Dighe, "Modeling stress state dependent damage evolution in a cast Al-Si-Mg aluminum alloy", *Theoretical and Applied Fracture Mechanics*, 33 (2000) 31-47.

610